Kovove Mater. 53 2015 415–422
DOI: 10.4149/km_2015_6_415

Cyclic oxidation behaviour of intermetallic Ti-46Al-8Ta alloy in air

T. Pelachová[1,2]*, J. Lapin[1]

[1] *Institute of Materials and Machine Mechanics, Slovak Academy of Sciences, Račianska 75, 831 02 Bratislava 3, Slovak Republic*
[2] *Faculty of Materials Science and Technology in Trnava, Slovak Technical University, Paulínska 16, 917 24 Trnava, Slovak Republic*

Received 26 August 2015, received in revised form 29 October 2015, accepted 30 October 2015

Abstract

The cyclic oxidation behaviour of intermetallic Ti-46Al-8Ta (at.%) alloy was studied in the air. Long-term oxidation experiments were carried out on the samples with convoluted type of γ(TiAl) + α_2(Ti_3Al) microstructure at temperatures ranging from 700 to 800 °C for oxidation time up to 3100 h. The oxidation kinetics was determined from the weight gain measurements as a function of oxidation time and temperature. The parabolic rate constants and activation energy for oxidation were calculated and discussed. The experimental results showed that the spallation had no significant effect on oxidation kinetic curves at 700 and 760 °C up to 3100 h but affected the measured kinetics at 800 °C for oxidation time longer than 500 h. The EDS and X-ray diffraction observations showed that the scales consisted of TiO_2, α-Al_2O_3, Ti_2AlN, TaAlTi and TiN phases.

K e y w o r d s: titanium aluminides, TiAl, cyclic oxidation, microstructure

1. Introduction

Titanium aluminides as attractive materials for high-temperature structural applications in automotive, aerospace and power industry have been extensively studied for more than twenty years [1, 2]. In recent years, different thermo-mechanical treatments and many different alloying additions have been explored to increase room temperature ductility, strength, high-temperature mechanical properties and also to improve high-temperature oxidation resistance of TiAl-based alloys [3–10]. Among various alloying elements, special attention was given to the effect of slow diffusing additions of Nb and Ta. The additions of Ta in air-hardenable TiAl-based alloys reduce significantly critical cooling rates needed for transformation of the α phase (Ti-based solid solution with hexagonal crystal structure) to massive γ_M [11]. Besides the effect of Ta on the microstructure refinement, several studies also reported its beneficial effect on high-temperature oxidation properties of some TiAl-based alloys during cyclic oxidation in air at temperatures ranging from 700 to 1000 °C [12–14]. Ta was found to be more effective in terms of increasing high-temperature oxidation resistance than Nb, particularly at 1000 °C [14]. Although all studies describe positive effect of Ta on oxidation resistance of TiAl-based alloys, the experimental results are limited to short oxidation time (up to 380 h) and oxidation kinetics lacks clear explanation due to a large fluctuation of experimental results. In addition, since the initial microstructure of intermetallic TiAl-Ta alloys has a significant effect on oxidation behaviour, various microstructure modifications can influence the oxidation kinetics. Hence, new studies on cyclic oxidation behaviour of TiAl-Ta alloys with an optimal microstructure designed for specific industrial applications are of large interest at temperatures corresponding to operating conditions and for long-term oxidation time.

The aim of this article is to study long-term cyclic oxidation behaviour of intermetallic Ti-46Al-8Ta (at.%) alloy with convoluted type of γ(TiAl) + α_2(Ti_3Al) microstructure at temperatures ranging from 700 to 800 °C in the air up to 3100 h. In addi-

*Corresponding author: tel.: +421 2 492 68 217; fax: +421 2 492 68 312; e-mail address: ummspela@savba.sk

tion, the mechanisms and kinetics of the oxidation are reported and discussed.

2. Experimental procedure

The Ti-46Al-8Ta (at.%) alloy was supplied in the form of cast and heat treated cylindrical bars with a diameter of 13 mm and length of 120 mm. Heat treatments consisted of hot isostatic pressing (HIP) at an applied pressure of 200 MPa, the temperature of 1260 ℃ for 4 h, which was followed by solution annealing at 1360 ℃ for 1 h and air cooling to room temperature. To obtain the convoluted microstructure, heat treatment was finalized by HIP ageing at an applied pressure of 150 MPa, the temperature of 1360 ℃ for 2 h followed by cooling at a rate of 5 ℃ min^{-1}. Cylindrical samples with a diameter of 10 mm and length of 15 mm for cyclic oxidation tests were cut from heat treated bars (HT). The surface of the samples was lathe machined, polished with 1 μm diamond paste and finally washed in acetone and dried. Cyclic oxidation tests were conducted in a resistance furnace at temperatures of 700, 760 and 800 ℃ and time from 2 h up to 3100 h under air. The samples were removed from the furnace at selected time intervals followed by air cooling for 15 min and then weighed using an analytical balance with an accuracy of ± 0.01 mg.

The microstructure evaluations of the oxide scales on the surface of the samples were performed by optical microscopy (OM), scanning electron microscopy (SEM), and backscattered scanning electron microscopy (BSEM). Samples for OM and SEM were prepared using standard metallographic techniques and etched in a solution of 150 ml H_2O, 25 ml HNO_3 and 10 ml HF. The oxidized samples were coated with a thin layer of Au before SEM examination. Distribution of elements in the scales was measured by energy-dispersive spectrometry (EDS) using JSM-7600F scanning electron microscope. Phase identification of the alloy and oxide scales was carried out by X-ray diffraction analysis (XRD) using Bruker D8 DISCOVER diffractometer equipped with X-ray tube with rotating Cu anode operating at 12 kW. All measurements were performed in symmetric mode. Diffraction patterns were registered within an angular range 20°–100° of 2θ with an exposition time of 2 s and a step size of 0.02°. The volume fraction of coexisting phases was determined from digitalized micrographs using the computer image software SigmaScan Pro.

3. Results and discussion

3.1. Microstructure of alloy

Figure 1 shows the typical fine grain structure of the heat treated Ti-46Al-8Ta (at.%) alloy. The grains are composed of γ(TiAl) and α_2(Ti_3Al) intermetallic phases. Figure 2 shows the convoluted type of $\gamma + \alpha_2$ microstructure consisting mostly of plate-like α_2 phase that forms small colonies within the γ phase. As shown by Lapin et al. [15], the α_2 lamellae and γ matrix within the colonies maintain the common Blackburn orientation relationship in the form $\{111\}\gamma \parallel (0001)\alpha_2$ and $[1\bar{1}0]\gamma \parallel [11\bar{2}0]\alpha_2$. A mean length and average volume fraction of the α_2 laths are measured to be 8.5 μm and (29.8 ± 2.3) vol.%, respectively. Besides the lamellar colonies, the microstructure of the alloy contains some single-phase α_2 and γ areas predominantly distributed along the grain boundaries.

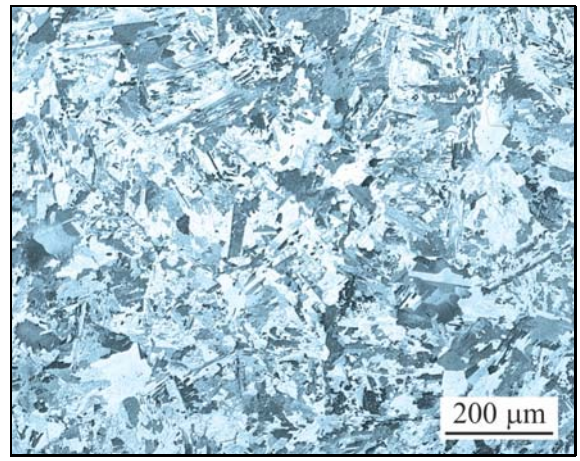

Fig. 1. OM showing fine grain structure of the heat treated Ti-46Al-8Ta (at.%) alloy.

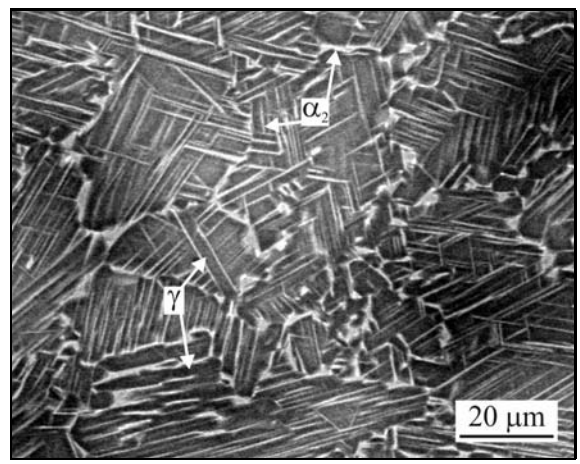

Fig. 2. BSEM micrograph showing the convoluted $\gamma + \alpha_2$ type of the microstructure.

3.2. Oxidation kinetics

Figure 3 shows measured weight gain Δm per unit area A of the samples as a function of oxidation time

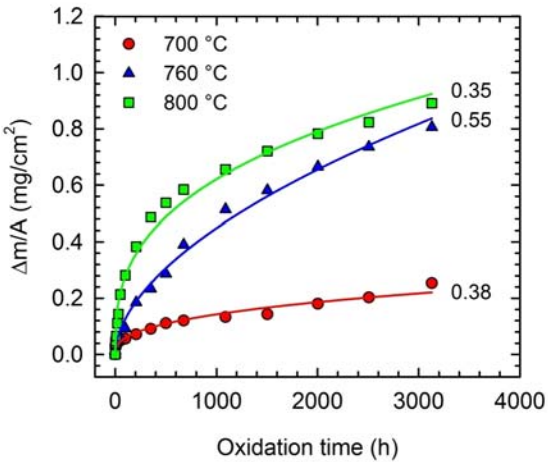

Fig. 3. Dependence of weight gain per unit area on the oxidation time. The studied temperatures are indicated in the figure.

at three studied temperatures of 700, 760 and 800 °C. As seen in this figure, the oxidation rate is found to increase with increasing temperature. To analyze the oxidation kinetics, the data was fitted to the power law rate equation:

$$\frac{\Delta m}{A} = (k_{\mathrm{p}} t)^{\frac{1}{n}}, \qquad (1)$$

where n is the exponent, k_{p} is the rate constant, and t is the oxidation time. Regression analysis of data shown in Fig. 3 leads to a power law exponent ranging from 0.35 to 0.55 which results in n ranging from 1.82 to 2.85. The correlation coefficients of these fits r^2 are better than 0.96. As shown by Mitoraj and Godlewska [12] for Ti-46Al-8Ta (at.%), Luo et al. [16] for Ti-46.5Al-3Ta-2Cr-0.2W (at.%) and Vojtěch et al. [14] for Ti-44.8Al-6.6Ta (at.%) alloys, early stages of the oxidation follow the linear kinetic model with a constant of $n = 1$ indicating that the forming oxidation scale is not protective. The similar sharp linear increase of the oxidation rate is also observed in the sample oxidized at 800 °C in the present work up to the oxidation time of about 10 h (Fig. 3). To investigate whether the oxidation kinetics obeys the parabolic law, the $(\Delta m/A)^2$ is plotted as a function of oxidation time in Fig. 4a. It is clear that the parabolic law approximately correlates with measured data at the temperatures of 700 and 760 °C up to the oxidation time of 3100 h. At the temperature of 800 °C, two regression lines with different slopes indicate a change of the oxidation kinetics of the alloy at the oxidation time of about 500 h. This change in the oxidation kinetics can be attributed mainly to spallation phenomena at 800 °C. It should be noted that only adhered scales of the samples were

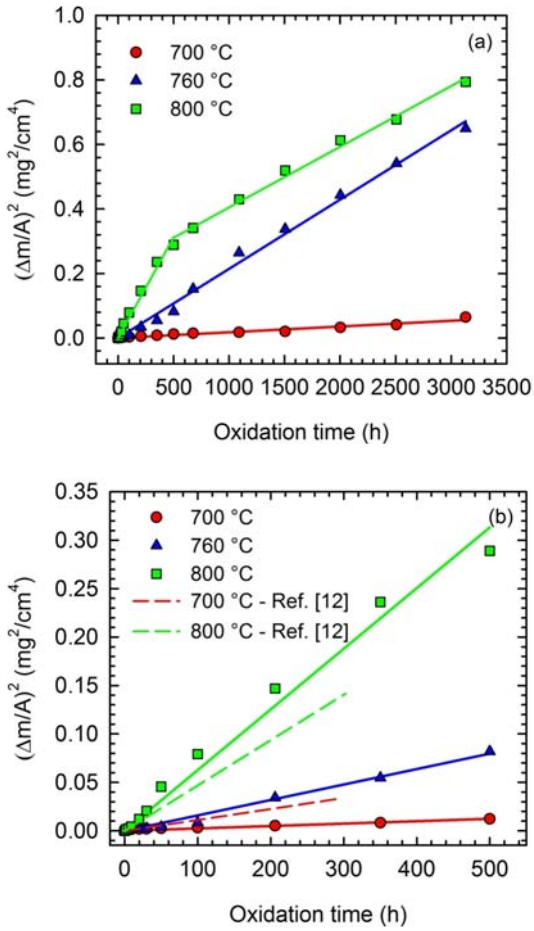

Fig. 4. Dependence of $(\Delta m/A)^2$ on oxidation time: (a) change of the oxidation kinetics at the temperature of 800 °C and oxidation time of 500 h; (b) detail showing comparison of the present work with the data published in the work [12] up to the oxidation time of 500 h. The studied temperatures are indicated in the figures.

measured during our experiment. Figure 4b shows a comparison of the dependence of $(\Delta m/A)^2$ on oxidation time obtained in the present work with the results of Mitoraj and Godlewska [12] for the Ti-46Al-8Ta (at.%) alloy. The experimentally obtained constants k_{p} for the studied alloy are summarized in Table 1. Since the experimental data taken from the work [12] are highly dispersed, the parabolic rate constants k_{p} are only estimated using regression analysis to be 3.136×10^{-14} and 1.301×10^{-13} g^2 cm^{-4} s^{-1} at 700 and 800 °C, respectively. While the value of $k_{\mathrm{p}} = 1.301 \times 10^{-13}$ g^2 cm^{-4} s^{-1} is comparable with that of 1.739×10^{-13} g^2 cm^{-4} s^{-1} in the present work at 800 °C, the value of 3.136×10^{-14} g^2 cm^{-4} s^{-1} differs by about one order of magnitude from that in the present work at 700 °C. The high fluctuation of data measured in the work [12] can be explained by a smaller surface of the oxidized samples, microstructural variations, laboratory air used during the exper-

Table 1. Experimentally obtained parabolic rate constants k_p at the temperatures of 700, 760 and 800 °C for studied alloy

Parabolic rate constant	Temperature		
	700 °C	760 °C	800 °C
k_p (g^2 cm^{-4} s^{-1})	6.854×10^{-15}	4.421×10^{-14}	1.739×10^{-13}

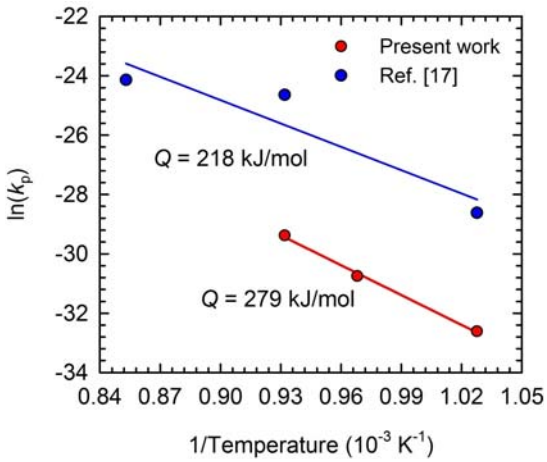

Fig. 5. Arrhenius type of diagram for the parabolic rate constant k_p as a function of inverse temperature.

iment, sample handling during cyclic oxidation experiments and measurements of the weight gain. Vojtěch et al. [14] studied high-temperature cyclic oxidation behaviour of the Ti-44.8Al-6.6Ta (at.%) alloy at 800–1000 °C. The regression analysis of the data measured at 800 °C in the work [14] leads to the values of $k_p = 1.294 \times 10^{-13}$ g^2 cm^{-4} s^{-1} and $k_p = 6.953 \times 10^{-13}$ g^2 cm^{-4} s^{-1} for the samples with adhered scales and the samples where spallation was included, respectively. The value of $k_p = 1.739 \times 10^{-13}$ g^2 cm^{-4} s^{-1} measured at 800 °C in the present work lies between these values and is comparable with the value of $k_p = 1.294 \times 10^{-13}$ g^2 cm^{-4} s^{-1} for the sample with adhered scales in the work [14]. It should be emphasized that the initial microstructure of Ti-44.8Al-6.6Ta (at.%) alloy [14] composed of $\gamma + \alpha_2$ lamellar grains and the grains with massive γ_M phase was significantly different from the convoluted type of microstructure of the studied Ti-46Al-8Ta (at.%) alloy.

The parabolic law indicates that the oxidation kinetics of the studied alloy is controlled by diffusion in the studied temperature range from 700 to 800 °C up to the oxidation time of 500 h. Assuming temperature dependence of the parabolic rate constant k_p in the form of Arrhenius type equation, Eq. (1) can be rewritten as follows:

$$\left(\frac{\Delta m}{A}\right)^2 = k_0 \exp\left(-\frac{Q}{RT}\right) t, \qquad (2)$$

where k_0 is a constant, Q is the activation energy for oxidation, R is the universal gas constant, and T is the temperature. Figure 5 shows Arrhenius type of diagram for the parabolic rate constant k_p as a function of inverse temperature. Taking the values of the parabolic rate constants shown in Table 1, one can calculate the activation energy for oxidation of $Q = (279 \pm 6)$ kJ mol^{-1}. This value is higher than that of 264 kJ mol^{-1} measured for oxidation of Ti-46.5Al-3Ta-2Cr-0.2W (at.%) alloy by Luo et al. [16] at temperatures between 800 and 900 °C or value of 218 kJ mol^{-1} reported by Godlewska et al. [17] for Ti-45.9Al-8Nb (at.%) alloy at temperatures ranging from 700 to 900 °C. However, the measured value of 279 kJ mol^{-1} is lower than the values of 404 and 295 kJ mol^{-1} measured for the activation energy for oxidation of binary TiAl and Ti_3Al, respectively, at temperatures ranging between 750 and 1000 °C. For the activation energy for self-diffusion of Ti and O in TiO_2, we can refer to the values of 257 and 234 kJ mol^{-1}, respectively [18]. For the activation energy for self-diffusion of Al and O in Al_2O_3, we can refer to the values ranging from 532 to 795 kJ mol^{-1} and from 281 to 482 kJ mol^{-1}, respectively, which were reported by Heuer [19]. The measured value of the activation energy for oxidation indicates that the oxidation process in Ti-46Al-8Ta (at.%) alloy is complex and is controlled not only by the diffusion of Ti and the diffusion of O through the oxide scale but also by the diffusion of other elements such as Ta, which can suppress TiO_2 growth [16].

3.3. Oxide scale morphology and composition

Figure 6 shows oxidized surface of the studied alloy with the typical morphology of oxide scales after selected regimes of oxidation. The short-term oxidation emphasizes the morphology of the initial $\gamma + \alpha_2$ microstructure up to the temperature of 760 °C and time of 25 h, as seen in Figs. 6a, 6b, and 6d. The oxidation time longer than 100 h and the oxidation at the temperature of 800 °C lead to the wane of the typical $\gamma + \alpha_2$ microstructural features, as shown in Figs. 6c and 6f–6l. In general, the oxide scales have good adherence to the alloy surface with quite limited spallation at all studied regimes. Figure 6 shows some cracks on the oxidized surfaces that could lead to spallation during the oxidation at 800 °C.

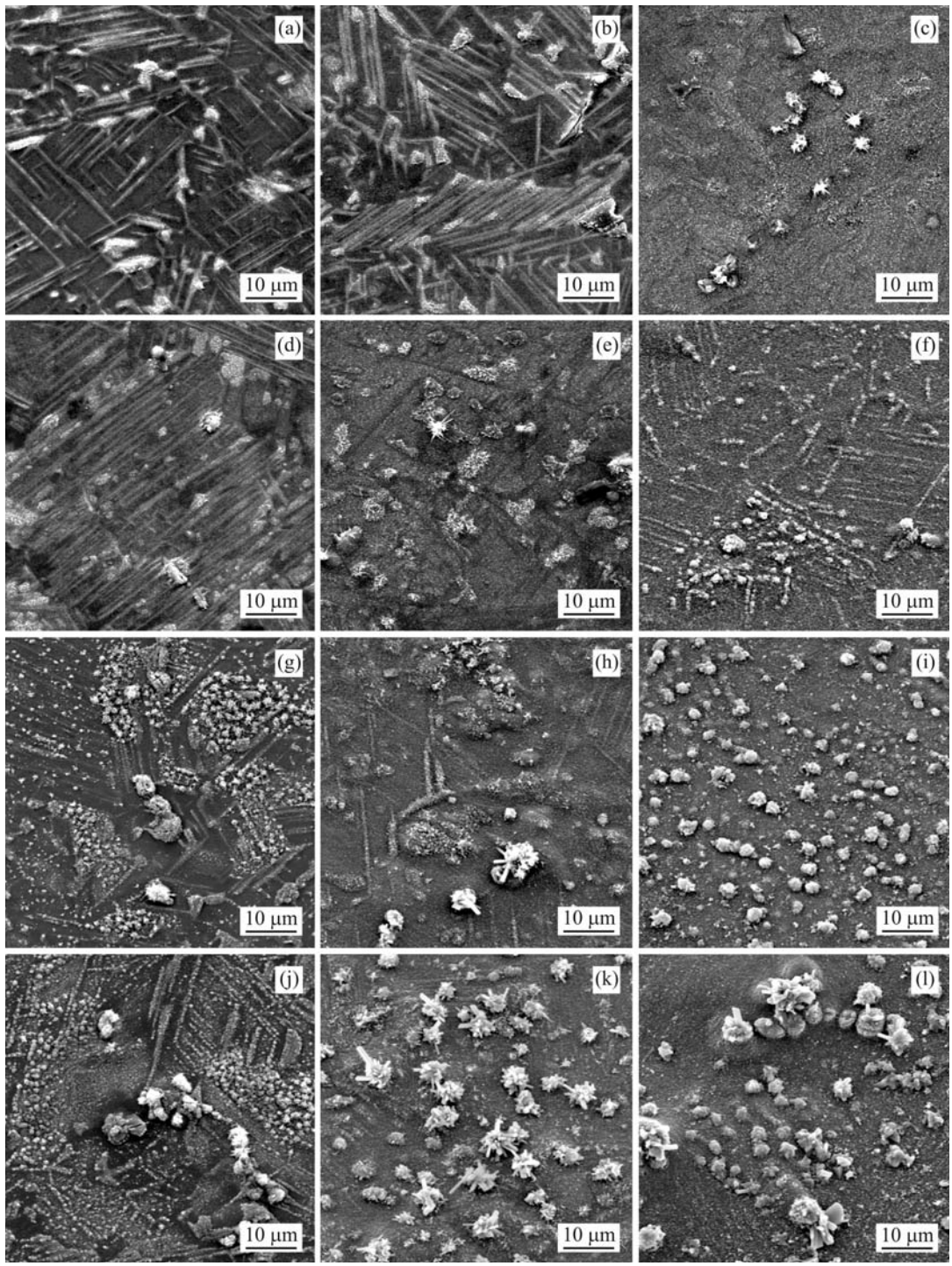

Fig. 6. SEM micrographs showing the surface of the Ti-46Al-8Ta (at.%) alloy after oxidation at 700, 760 and 800 °C for different oxidation time: (a, b, c) 25 h, (d, e, f) 100 h, (g, h, i) 1000 h and (j, k, l) 2000 h.

Figure 7 shows phase composition of the alloy surfaces before (HT) and after cyclic oxidation in air using X-ray diffraction. As shown in Fig. 7a, the XRD spectra belong mainly to the basic intermetallic phases of the alloy (TiAl and Ti_3Al) after oxidation for 25 h. Reflections of TiO_2 (rutile) can be clearly visible on XRD spectra after the oxidation for 25 h at all studied temperatures. The higher temperature, the stronger TiO_2 reflections. On the other hand, no clear reflections of α-Al_2O_3 (corundum) phase are visible after the oxidation for 25 h. In addition, weak diffraction peaks of TiN phase are also identified. The XRD spectra measured for the time of 100 h and longer indicate the growth of the oxide scales with the increasing

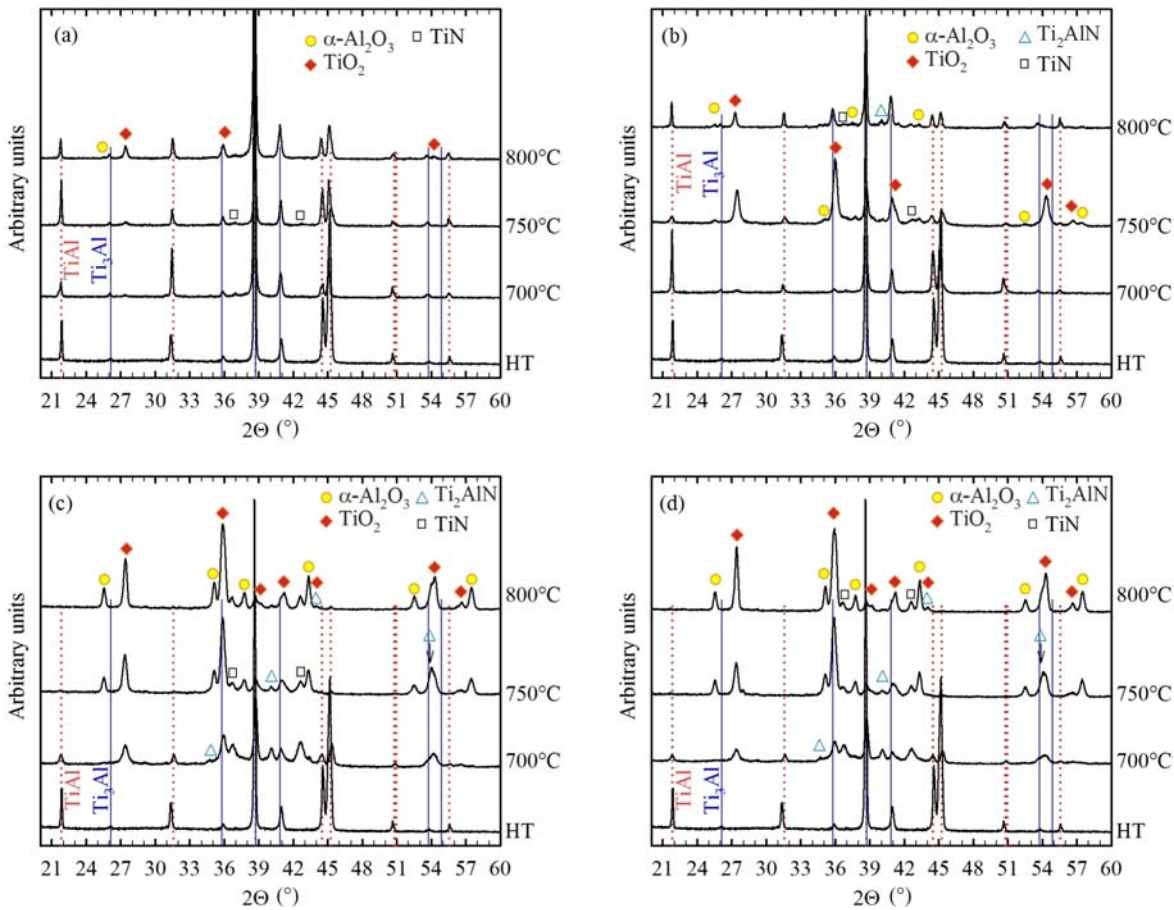

Fig. 7. XRD spectra of the as-received samples (HT) and the samples after oxidation at 700, 760 and 800 °C with duration of (a) 25 h, (b) 100 h, (c) 1000 h and (d) 2000 h.

temperature and time that results in a decrease of the diffraction intensity of the TiAl and Ti_3Al phases, as shown in Figs. 7b, 7c and 7d. At the temperatures of 760 and 800 °C, the Al_2O_3 and TiO_2 phases are identified as the typical oxidation products. The diffraction maxima of other phases, such as Ti_2AlN and TiN are also present on the scale. The same oxidation products were reported in the work [12] after 300 h oxidation at the temperatures of 700 and 800 °C. The XRD spectra after the oxidation for 1000 and 2000 h provide clear diffraction maxima shown in Figs. 7c and 7d. The phase analysis showed the same phase composition of the oxide scales as was formed at the shorter time of oxidation.

Figure 8 shows the distribution of elements and elemental line profiles across the scale and sub-scale zone measured by EDS for the sample oxidized at 800 °C for 1000 h. SEM micrograph clearly indicates several phases in the scale, as shown in Fig. 8a. Figures 8b and 8c indicate that Al-O oxide, which is identified to belong to Al_2O_3 is formed in the continuous outer part of the scale and at the interface between the alloy and the scale. The central part of the scale contains Ti-O type of oxide (Fig. 8d) which belongs to TiO_2. The central TiO_2 layer is decorated by numerous Ta-rich particles, as seen in Fig. 8e. Mitoraj and Godlewska [12] found the same Ta-rich particles in this alloy after cyclic oxidation in air for 300 h at 800 °C and described them as TaAlTi phase. Figure 8f shows the concentration profiles along the line 1 in Fig. 8a. The high concentration of Ti with missing oxygen next to Ta-rich particle could be the TiN phase that was detected by XRD. Comparing the EDS profiles with XRD spectra it can be concluded that the major components of the consecutive layers, starting from the alloy surface are: the mixed scale of Al_2O_3 and TaAlTi particles, TiN, TiO_2, and Al_2O_3. It should be noted that the composition of the scales after 1000 h cyclic oxidation at 800 °C is qualitatively the same as that observed after 300 h oxidation at 800 °C by Mitoraj and Godlewska [12], which growth obeys the parabolic law.

4. Conclusions

The investigation of the long-term cyclic oxidation behaviour of intermetallic Ti-46Al-8Ta (at.%) alloy in the air at temperatures of 700, 760 and 800 °C suggests

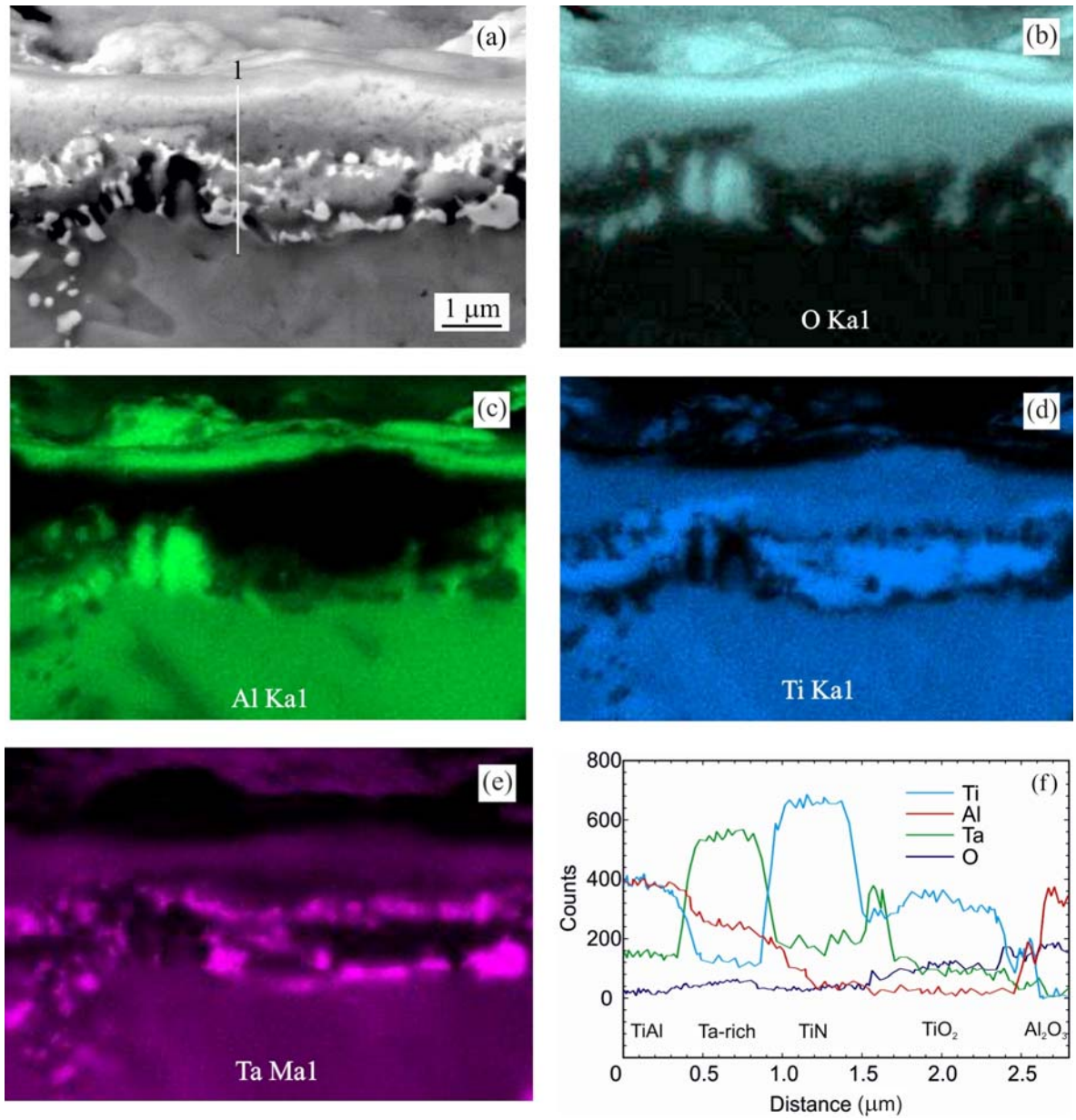

Fig. 8. Cross section of the oxide scale in sample oxidized at 800 °C for 1000 h with EDS maps and line profiles: (a) SEM micrograph, (b) distribution of oxygen, (c) distribution of Al, (d) distribution of Ti, (e) distribution of Ta, (f) EDS line profiles of the elements across the oxide scale and sub-scale zone through the line 1 shown in 6a.

the following conclusions:

1. The oxidation kinetics measured by the weight gain per unit area of the samples as a function of oxidation time and temperatures follows the power law with the measured exponent n ranging from 1.82 to 2.85 over the studied temperature range.

2. Assuming the parabolic law for oxidation and experimentally measured parabolic rate constants in the temperature range from 700 to 800 °C up to the oxidation time of 500 h, the activation energy for oxidation is calculated to be 279 kJ mol^{-1}.

3. Starting from the upper surface of the oxidized samples, the major components of the oxide layers are identified by X-ray diffraction and EDS to be Al_2O_3 and TaAlTi particles, TiN, TiO_2, Ti_2AlN, and Al_2O_3.

Acknowledgements

This work is based on the results of the project Competence center for new materials, advanced technologies and energy ITMS 26240220073, supported by the Research and Development Operational Program funded by the European Regional Development Fund and on the results of the project Center for Applied Research of New Materials and Technology Transfer, ITMS 26240220088,

supported by the Science and Research Operational Program by the European Regional Development Fund.

The authors would like to thank E. Dobročka from the Institute of Electrical Engineering of the Slovak Academy of Sciences for XRD measurements.

References

[1] Wu, X.: Intermetallics, *14*, 2006, p. 1114. doi:10.1016/j.intermet.2005.10.019

[2] Bolz, S., Oehring, M., Lindermann, J., Pyczak, F., Paul, J., Stark, A., Lippmann, T., Schrüfer, S., Roth-Fagaraseanu, D., Schreyer, A., Weiß, S.: Intermetallics, *58*, 2015, p. 71. doi:10.1016/j.intermet.2014.11.008

[3] Zhang, W., Lorentz, U., Appel, F.: Acta Mater., *48*, 2000, p. 2803. doi:10.1016/S1359-6454(00)00093-8

[4] Wang, J. N., Xie, K.: Intermetallics, *8*, 2000, p. 545. doi:10.1016/S0966-9795(99)00153-3

[5] Novoselova, T., Malinov, S., Sha, W.: Intermetallics, *11*, 2003, p. 491. doi:10.1016/S0966-9795(03)00028-1

[6] Liu, B., Liu, Y., Huang, L., Li, H., He, Y.: Mater. Charact., *105*, 2015, p. 113. doi:10.1016/j.matchar.2015.05.008

[7] Shu, S., Qiu, F., Tong, C., Shan, X., Jiang, Q.: J. Alloy. Compd., *617*, 2014, p. 302. doi:10.1016/j.jallcom.2014.07.199

[8] Beddoes, J., Chen, W. R., Zhao, L.: J. Mater. Sci., *37*, 2002, p. 621. doi:10.1023/A:1013786028136

[9] Larson, D. J., Liu, C. T., Miller, M. K.: Mat. Sci. Eng. A, *270*, 1999, p. 1. doi:10.1016/S0921-5093(99)00233-6

[10] Cheng, T. T., Willis, M. R., Jones, I. P.: Intermetallics, *7*, 1999, p. 89. doi:10.1016/S0966-9795(98)00016-8

[11] Saage, H., Huang, A. J., Hu, D., Loretto, M. H., Wu, X.: Intermetallics, *17*, 2009, p. 32. doi:10.1016/j.intermet.2008.09.006

[12] Mitoraj, M., Godlewska, E. M.: Intermetallics, *34*, 2013, p. 112. doi:10.1016/j.intermet.2012.10.014

[13] Godlewska, E., Mitoraj, M., Leszczynska, K.: Corros. Sci., *78*, 2014, p. 63. doi:10.1016/j.corsci.2013.08.032

[14] Vojtěch, D., Popela, T., Kubásek, J., Maixner, J., Novák, P.: Intermetallics, *19*, 2011, p. 493. doi:10.1016/j.intermet.2010.11.025

[15] Lapin, J., Pelachová, T., Dománková, M.: Intermetallics, *19*, 2011, p. 814. doi:10.1016/j.intermet.2010.11.023

[16] Luo, Y., Zeng, W., Xi, Z., Mao, X., Yang, Y., Wu, J., Su, H.: Rare Metal Mat. Eng., *44*, 2015, p. 282. doi:10.1016/S1875-5372(15)30020-5

[17] Godlewska, E., Mitoraj, M., Devred, F., Nieuwenhuys, B. E.: J. Therm. Anal. Calorim., *88*, 2007, p. 225. doi:10.1007/s10973-006-8291-x

[18] Velasco, B. G., Aswath, P. B.: J. Mater. Sci., *33*, 1998, p. 2203. doi:10.1023/A:1004395908966

[19] Heuer, A. H.: J. Eur. Ceram. Soc., *28*, 2008, p. 1495. doi:10.1016/j.jeurceramsoc.2007.12.020